



Combining Multifrequency Microwave and Optical Data for Crop Management

M. S. Moran,* A. Vidal,[†] D. Troufleau,[†] J. Qi,* T. R. Clarke,*
P. J. Pinter, Jr.,* T. A. Mitchell,* Y. Inoue,[‡] and C. M. U. Neale[§]

The potential for the combined use of microwave and optical data for crop management is explored with the use of images acquired in the visible, near-infrared, and thermal spectrum and the synthetic aperture radar (SAR) wavelengths in the Ku (14.85 GHz) and C (5.3 GHz) bands. The images were obtained during June 1994 and covered an agricultural site composed of large fields of partial-cover cotton, near-full-cover alfalfa, and bare soil fields of varying roughness. Results showed that the SAR Ku backscatter coefficient (Ku-band σ^0) was sensitive to soil roughness and insensitive to soil moisture conditions when vegetation was present. When soil roughness conditions were relatively similar (e.g., for cotton fields of similar row direction and for all alfalfa fields), Ku-band σ^0 was sensitive to the fraction of the surface covered by vegetation. Under these conditions, the Ku-band σ^0 and the optical normalized difference vegetation index (NDVI) were generally correlated. The SAR C backscatter coefficient (C-band σ^0) was found to be sensitive to soil moisture conditions for cotton fields with green leaf area index (GLAI) less than 1.0 and alfalfa fields with GLAI nearly 2.0. For both low-GLAI cotton and alfalfa, C-band σ^0 was correlated with measurements of surface temperature (T_s). A theoretical basis for the relations between Ku-band σ^0 and NDVI and between C-band σ^0 and T_s was presented and supported with on-site measurements.

On the basis of these findings, some combined optical and radar approaches are suggested for crop management applications. ©Elsevier Science Inc., 1997

INTRODUCTION

The potential of optical remote sensing for crop management has been established through a multitude of studies in the past 25 years. Measurements of reflected and emitted energy from vegetated surfaces have been used for such important farm applications as scheduling irrigations, predicting crop yields, and detecting certain plant diseases and insect infestations (Jackson, 1984). The basic physics behind these successful applications is well known.

In the reflective region of the optical spectrum, discrimination of crop growth and plant status is generally accomplished by computing a ratio or linear combination of visible and near-infrared reflectances, termed a vegetation index (VI). One of the more commonly used VIs is the normalized difference vegetation index (NDVI) (Rouse et al., 1974):

$$\text{NDVI} = (\rho_{\text{NIR}} - \rho_{\text{Red}}) / (\rho_{\text{NIR}} + \rho_{\text{Red}}), \quad (1)$$

where ρ_{NIR} and ρ_{Red} are the reflectance of the surface in the near-infrared (NIR) and red spectrum, respectively. NDVI has been found to be sensitive to such vegetation parameters as the green leaf area index (GLAI), the fraction absorbed photosynthetically active radiation, and the percentage of the ground surface covered by vegetation (V_c). This sensitivity is attributed to the absorption of incident red radiation by plant chlorophyll and scattering of incident NIR radiation by plant leaf structure (Jackson and Huete, 1991). For surfaces only partially covered by vegetation, the NDVI can be perturbed by differences in soil brightness due to variations in soil roughness or moisture content (Huete, 1988).

* USDA-ARS U. S. Water Conservation Laboratory, Phoenix, Arizona

[†] Cemagref-ENGREF Remote Sensing Research Laboratory, Montpellier, France

[‡] NIAES Laboratory of Agro-Biological Measurements, Tsukuba, Japan

[§] Department of Biological and Irrigation Engineering, University of Utah, Logan

Address correspondence to Dr. Susan Moran, USDA-ARS U.S. Water Conservation Laboratory, 2000 E. Allen Road, Tucson, AZ 85719.

Received 15 January 1996; revised 30 July 1996.

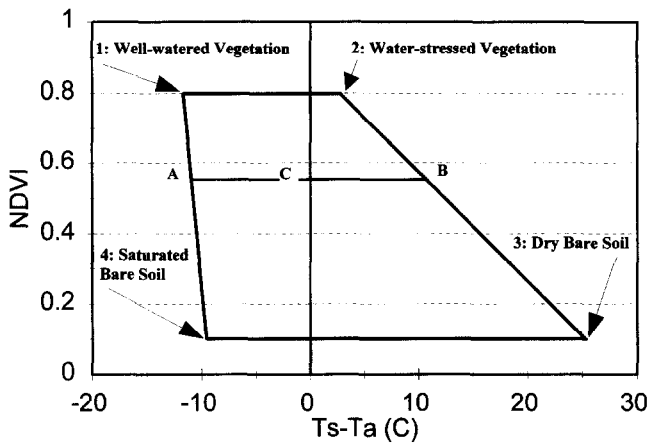


Figure 1. The trapezoidal shape of the vegetation index–temperature relation for cotton at Maricopa Agricultural Center (MAC) on day-of-year 165, based on meteorological conditions and theoretical considerations outlined by Moran et al. (1994). The water deficit index is equal to the ratio of AC/AB and ranges from 0 for a well-water crop to 1 for a crop under extreme water stress.

In the thermal region, remotely sensed measurements of soil and foliage temperature have been linked to soil moisture content, plant water stress, and plant transpiration rate (Jackson, 1982; Tanner 1963). Algorithms based on remotely sensed surface temperature (T_s) have been developed to assess soil salinity, soil waterlogging, plant water potential, and photosynthesis, as well as final crop yield [see historical reviews by Jackson (1987) and Idso et al., (1986)]. The sensitivity of surface temperature to plant and soil moisture conditions is related primarily to the heat loss associated with evaporation and transpiration. As such, the thermal signal is related to the percentage of the site covered by vegetation and the water status of the vegetation and soil (i.e., evapotranspiration, or ET). The thermal signal is generally interpreted in relation to such meteorological conditions as air temperature (T_a), incoming solar radiation ($R_{s\downarrow}$), vapor pressure deficit (VPD) and wind speed (U).

Even when T_a , $R_{s\downarrow}$, VPD, and U are constant (e.g., for a local area at one time of day), the sensitivity of the thermal signal to ET rate is still confounded by variations in V_c . Thus, attempts have been made to combine NDVI and T_s in a single index related to the water status of the plants and soil in the field (Hope, 1988; Nemani and Running, 1989; Price, 1990). As the NDVI increases, the range of possible $T_s - T_a$ values for a given range of ET rates decreases, resulting in a trapezoidal vegetation index–temperature (VIT) shape (Fig. 1). With the use of theoretical methods to define the edges of the VIT trapezoid (Carlson et al., 1994; Moran et al., 1994), it is possible to compute a single water deficit index (WDI) defined by the ratio of AC/AB in Figure 1. The WDI has been found to be useful for such farm management ap-

plications as irrigation scheduling (Moran, 1994) and forest fire prediction (Vidal and Devaux-Ros, 1995).

Although optical remote sensing provides a powerful farm management tool, there are some serious limitations that have restricted farm management applications. Because energy in the optical region cannot penetrate clouds, the acquisition of optical images for farm management is limited to periods of cloud-free sky conditions. Even when clouds are absent, the optical signal is highly sensitive to atmospheric scattering and absorption and requires correction for atmospheric effects for multi-temporal applications. Furthermore, care must be taken regarding the time of acquisition because both surface reflectance and temperature are a function of the solar illumination angle (Lagouarde et al., 1995; Qi et al., 1995). These limitations are serious for farm management applications in which quantitative information is needed on a daily basis with a turnaround time of hours.

An alternative to the use of optical remote sensing for farm management is the use of radar backscattering data. The radar backscatter signal (σ^0) is expressed as the sum of the contribution of the vegetation layer (σ_v^0) and the contribution of the soil (σ_s^0), the latter attenuated through the vegetation (Attema and Ulaby, 1978). That is,

$$\sigma^0 = \sigma_v^0 + \tau^2 \sigma_s^0 \quad (\text{m}^2/\text{m}^2), \quad (2)$$

where τ^2 is the two-way attenuation through the vegetation. The scattering behavior of the radar signal is governed by both the dielectric properties of the soil and vegetation and the geometric configuration of the scattering elements (soil roughness, leaves, stalk, and fruit) with respect to the wavelength, direction, and polarization of the incident wave. Synthetic aperture radar (SAR) systems have the advantages of cloud penetration and high spatial resolution (on the order of 30 m from current satellite systems). Because the SAR sensor provides its own illumination source, acquisitions may be obtained during the day and night, and the signal is independent of the solar illumination angle. On the other hand, σ^0 is a function of the wavelength, polarization, and incidence angle of the illumination source (Brisco et al., 1990; Brown et al., 1992; Fung and Chen, 1992; Poirier et al., 1988).

There is some evidence that the radar signal at high frequencies is particularly sensitive to such plant parameters as GLAI, plant biomass, and percentage of vegetation cover (Bouman, 1991; Prevot et al., 1993). Ulaby et al. (1984) reported that the temporal variations in σ_v^0 at 13 GHz could be accounted for through variations in green leaf area alone, for GLAI values greater than 0.5. However, they also found that the Ku signal was very sensitive to soil roughness (particularly at scales of ~ 2 cm) and, for $\text{GLAI} < 0.5$, the backscatter could be affected by soil moisture conditions. Furthermore, for $\text{GLAI} > 2.0$, σ_v^0 at Ku frequency remained relatively con-

stant, though the GLAI increased to values as high as 5 and 6 for corn and sorghum.

At lower frequencies, there is evidence that the backscatter signal is very sensitive to soil moisture (Benallegue et al., 1994; Bertuzzi et al., 1992; Dabrowska-Zielinska et al., 1994; Lin et al., 1994; Schmillius and Furrer, 1992a). The soil backscatter coefficient is dominated by the dielectric properties of the surface. Because the dielectric constant of water (below 10 GHz) is about 80 and that of dry vegetation or soil is about 2–3, the backscatter signal of low-frequency radar is highly sensitive to the amount of soil moisture. However, it is apparent from Eq. (2) that the low frequency signal can be attenuated by increasing vegetation cover, thus decreasing its sensitivity to soil moisture conditions (Schmillius and Furrer, 1992b). These complications have restricted the use of radar data for mapping soil moisture conditions of heterogeneous, natural landscapes. However, these complications are less restrictive for farm management applications where field conditions are generally well known (e.g., planting date, crop type, soil cultivation practices, etc.).

On the basis of the results of previous studies, it would appear that the high-frequency radar data (~ 13 GHz) and the optical vegetation index are both sensitive to GLAI and percentage of vegetation cover and could possibly be used interchangeably (Benallegue et al., 1994; Daughtry et al., 1991; Prevot et al., 1993). It also appears that low-frequency (~ 5 GHz) radar backscatter and surface temperature are both sensitive to soil moisture for sparsely vegetated fields and to plant transpiration rates for dense vegetation (Soares et al., 1987; Trouffleau et al., 1996). Just as the interpretation of $T_s - T_a$ is confounded by variations V_c (Fig. 1), so also the sensitivity of C-band σ^0 to soil moisture is diminished with increasing vegetation [Eq. 2]. A preliminary analysis of this hypothesis was made by combining high- and low-frequency radar data sets with a modeling approach (Prevot et al., 1993) to construct a mesh graph, whose cartesian coordinates were related to soil water and crop growth conditions, respectively (Fig. 2) (Moran et al., 1996c). The striking similarities between the graphs in Figures 1 (optical data) and 2 (SAR data) illustrate the potential for interchanging optical and SAR data for farm management. However, the physical mechanisms that underlie these relations are very different for the optical and microwave spectrum, and the sensitivity of the signal to the surface conditions and the limitations of the application also differ (Engman, 1991).

In this study, we explored the potential information and limitations of radars operating in two microwave bands (Ku band at 14.85 GHz, VV, incidence angle 55° ; C band at 5.3 GHz, VV, incidence angle 23°) for farm management applications. These radar configurations were chosen owing to the availability of such data, using existing instruments aboard aircraft or satellite (Table 1).

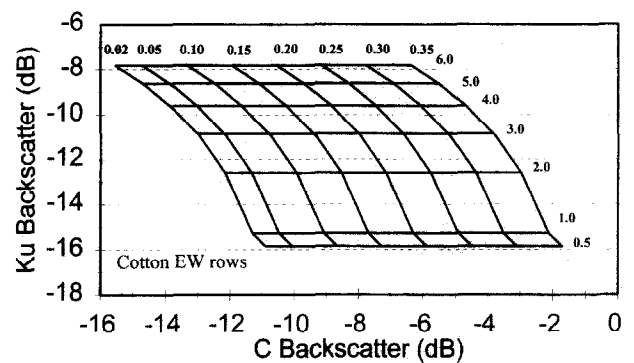


Figure 2. The mesh graph of Ku- and C-band backscatter based on the multispectral-airborne-demonstration-at-MAC measurements and simulation modeling of a cotton crop with east-west (EW) rows at MAC (Moran et al., 1996c). The solid lines define modeled backscatter for values of GLAI (listed at the right) and volumetric soil moisture (listed at the top).

The sensitivity of these data to field characteristics was compared with that of optical data (surface reflectance and temperature) for the same fields and dates. An empirical analysis and a theoretical justification are presented.

DATA SETS

The multispectral airborne demonstration at Maricopa Agricultural Center (MADMAC) experiment was conducted during the cotton growing season from April through October 1994 (Moran et al., 1996a). The site for the experiment was MAC, a 770-ha research and demonstration farm located about 48 km south of Phoenix, owned and operated by the University of Arizona. The demonstration farm is composed of large fields (up to 0.27×1.6 km) used for demonstrating new farming techniques on a production scale. Alfalfa is grown year-round with about seven or eight harvests per year; cotton is grown during the summer, and wheat during the winter. A data management system is in place to archive planting and harvesting information, as well as the times and amounts of water, herbicide, and pesticide applications. Because the predominant irrigation method for the MAC demonstration farm is flooding, each field is dissected into level-basin "borders." During a single irrigation, the borders are sequentially flooded with a 3–4 day progression from one end of a 1.6-km field to the other.

The objective of MADMAC was to investigate the utility of multispectral remotely sensed data for day-to-day farm management. Images of MAC were acquired in four spectral wavelength bands (green, red, NIR and thermal) about every 2 weeks by using airborne cameras flown at two altitudes (1200 and 2300 m) above ground level (AGL) (Neale and Crowther, 1994). During each overpass, a survey of the farm was conducted to record

Table 1. Optical and Radar Sensors and Sensor Specifications and Details about Deployment at MAC during June 1994

Sensor	Platform	Specifications	Overflight
Utah State University	Piper Seneca II 1200 m AGL 2400 m AGL	2-m pixel (reflective bands) 4-m pixel (thermal band) 4 bands: (10 nm wide) Green: 0.55 μm Red: 0.65 μm NIR: 0.85 μm TIR: 8–12 μm	15 June 1994, DOY 165, about 11:00 A.M.
Daedalus	Lockheed P-3A 1500 ft AGL	1-m pixel 6 bands: Green 0.52–0.60 μm Red 0.63–0.69 μm NIR 0.76–0.90 μm NIR 0.91–1.05 μm MIR 3.0–5.5 μm TIR 8.5–12.5 μm	24 June 1994, DOY 175, about 11:00 A.M.
SAR	ERS-1 in orbit	6-looks format from CCRS Spatial resolution: 35 m Pixel spacing: 12.5 m C band: 5.3 GHz Polarization: VV Incidence angle: 23°	15 June 1994, DOY 165, about 10:00 P.M.
SAR	Lockheed P-3A 15,000 ft AGL	Spatial resolution: 1 m Ku band: 14.85 GHz Polarization: VV Incidence angle: 55°	24 June 1994, DOY 175, about 11:00 A.M.

Abbreviations: AGL, above ground level; MIR, (middle infrared); TIR, (thermal infrared); CCRS, Canadian Centre for Remote Sensing.

border-by-border estimates of crop height, V_c , phenologic stage, soil roughness, and soil moisture. In selected fields, detailed measurements were made of such crop properties as density, biomass, and GLAI. In a 10-day period in June 1994, we arranged to obtain SAR images in the Ku and C wavelengths concurrent with acquisitions of images of surface reflectance and temperature (Table 1). This subset of the MADMAC data is the subject of the analysis presented here. The processing of the spectral and agronomic data is addressed in the following sections.

Spectral Data

The European remote sensing (ERS-1) satellite supports an imaging SAR sensor operating at C band (5.35 GHz), VV polarization, and 23° incidence angle. A SAR image covering most of MAC was obtained on 15 June during an ascending pass at about 10:00 P.M. MST. The digital numbers (dns) were converted into a backscattering coefficient expressed in decibels by using the SAR calibration coefficient, $X_c=63.8$, provided by the Canadian Centre for Remote Sensing (CCRS, personal communication). According to CCRS, X_c is "approximate"; however, the accuracy of the calibration coefficient was not crucial to this work, because we did not use multirate images.

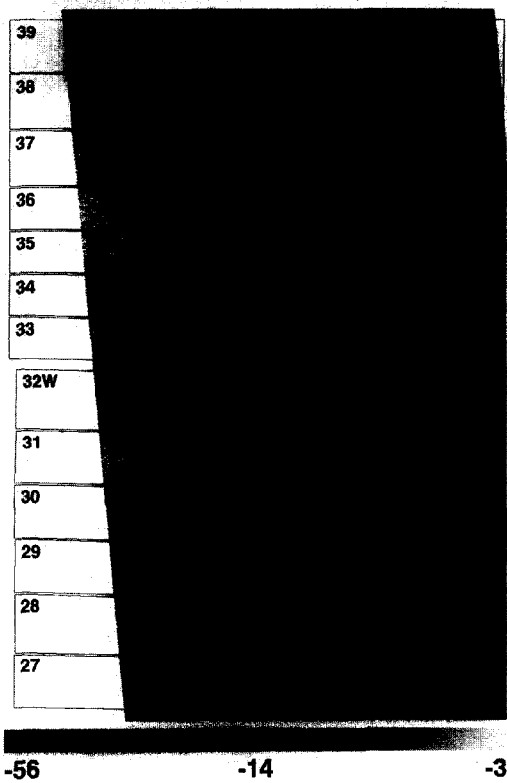
Sandia National Laboratories (SNL) in Albuquerque, New Mexico, provided an airborne imaging SAR sensor operating at Ku band (14.85 GHz), VV polarization, and 55° incidence angle. A SAR image covering most of MAC

was obtained on 24 June at 11:00 A.M. MST (Fig. 3). The SAR dn was expressed in decibels based on the calibration coefficient, $X_k=0.001526$ (J. Bradley, SNL, personal communication), with an estimated calibration error of 1.2 dB.

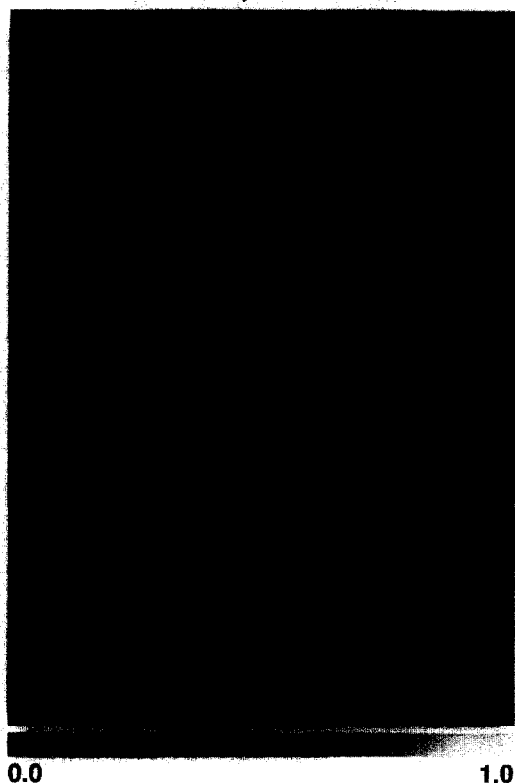
EG&G Energy Measurements, Inc., in Las Vegas, Nevada, provided an airborne Daedalus imaging system with six spectral bands ranging from the visible to thermal spectral region. This sensor was mounted in the same aircraft with the Sandia SAR instrument, passing over MAC on 24 June at 11:00 A.M. MST (Fig. 3). On the basis of calibration coefficients provided by EG&G (C. Golanics, personal communication), the dns were converted into radiance (W/m^2). Using 25' \times 25' calibration panels of 0.08 and 0.64 reflectance and on-site measurements of T_s in selected fields, we converted the images of at-sensor radiance into images of surface reflectance and temperature.

Scientists from Utah State University (USU) deployed a multispectral airborne video system with four spectral bands covering the visible to thermal spectral region on 15 June at 11:00 A.M. Video frames were mosaicked on a field-by-field basis to produce whole images of the farm. Similar to the processing of the Daedalus data, the USU images were converted from voltage into surface reflectance and temperature by using the correlation between voltage values, as well as known surface reflectances and temperatures within the scene (on-site measurements and calibration panels).

MAC Ku-band SAR Backscatter, 24 June 1994



MAC NDVI, 24 June 1994



MAC Surface Temperature, 24 June 1994

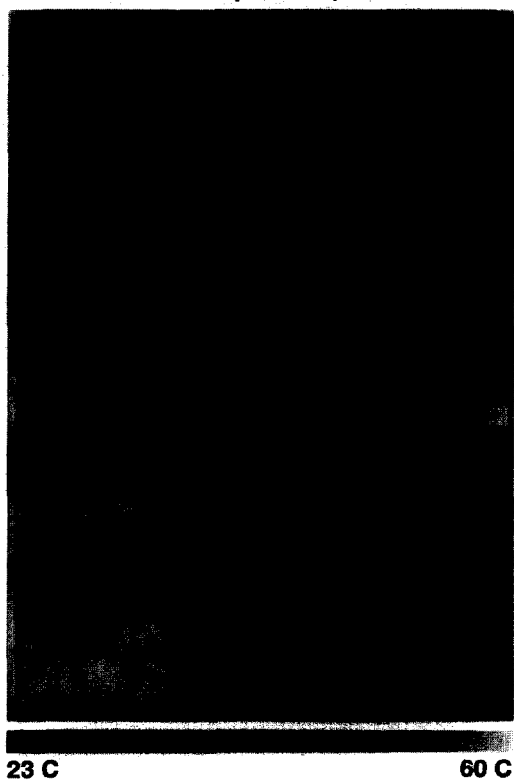


Figure 3. Images of MAC acquired with the airborne multipod system (AMPS) on 24 June 1994, processed to SAR Ku backscatter (dB), NDVI, and surface temperature ($^{\circ}$ C).

Table 2. MAC Field Conditions According to the Visual Field Survey Conducted on DOY 165

Field no.	Crop Type	Soil Roughness	Vegetation Height (mm)	Vegetation Cover (%)	Soil Moisture
11	Cotton	NS rows, raked	B1-3: 8	B1-3: 45	Moist
13	Cotton	NS rows, raked	B1-6: 8 B7-8: 6	B1-2: 60 B3-8: 50	B1: moist B2-8: wet
15	Alfalfa	Smooth	B1-16: 5	B1-16: 80	B1: wet B2-16: water
17	Alfalfa	Smooth	B1-16: 5	Ranging from 80% in B16 to 30% in B2	B1-6: wet B7-10: moist B11-16: damp
19	Cotton	NS rows, raked	B1: 7 B2-4: 6	B1: 40 B2-4: 35	Dry
20	Cotton	NS rows, raked	B1-3: 5 B4: 6	B1-3: 25 B4: 35	Dry
23	Cotton	NS rows, smooth	B1-4: 8	B1: 40 B2: 20 B3: 30 B4: 50	Dry
25	Alfalfa	Smooth	B1-16: 5 mm	50% in B2; 70-80% in all other borders	B1-5: moist B6-9: wet B10-16: moist
31	Cotton	EW rows, raked	B1-8: 7	B1-8: 40	Dry
33	Cotton	EW rows, raked	B1-4: 5	B1-4: 35	Dry
34	Cotton	EW rows, raked	B1: 6 B2-4: 7	B1: 25 B2-4: 35	Dry
35	Cotton	EW rows, raked	B1, B3, B5, B7: 6 All others: 3	B1, B3, B5, B7: 30 All others: 10	B1: water B2-B7: moist
36	Cotton	EW rows, raked	B3: 4 All others: 6	B3: 15 All others: 30	B1-3: dry B4-7: moist
37	Cotton	EW rows, raked	B1-3: 6 B4: mix	B1-3: 30 B4: Mix	Moist
38	Cotton	EW rows, raked	B1, B4: 7 B2, B3: 6	B1, B4: 35 B2, B3: 25	Dry
39	Lesquerella (B1-8, B13-16) Barren (B9-12)	B1-8, B13-16: smooth; B9-12: cultivated	Unknown	B1-8, B13-16: varied from 10-50%	Dry

Abbreviations: B, border; EW, east-west; NS, north-south.

For each field border, values of T_s , ρ_{NIR} , and ρ_{Red} from the EG&G and USU sensors and values of C-band σ^0 and Ku-band σ^0 from the ERS-1 and SNL sensors were computed by averaging the values for all pixels located within the border. The number of pixels averaged varied with the size of the border. For the coarsest-resolution data, ERS-1 SAR (30-m pixels), the number of pixels averaged ranged from 14 pixels for the smallest border to nearly 100 pixels for the largest. For the finest resolution data, SNL SAR (1-m pixels), the number of pixels averaged for each border was well over 1000.

Agronomic and Edaphic Measurements

During each USU overpass, a survey of the farm was conducted to record border-by-border estimates of crop height, V_c , soil roughness, and soil moisture. The survey results for 15 June [day of year (DOY) 165] are included in Table 2 for the fields used for this study. In addition to the visual surveys, detailed vegetation measurements were made in selected cotton and alfalfa fields on a weekly basis during MADMAC. In the sample sites

within the cotton fields, measurements were made of plant density, height, V_c , and number of squares/bolls/flowers. Five plants were weighed in each sample site, and the plant of median weight was taken to the laboratory for measurement of wet and dry biomass and GLAI. The weight of the wet biomass was measured immediately; dry biomass weight was measured after at least 48 h in an oven at 68°C; and GLAI was measured by using a light-sensitive leaf area meter. In sample sites within the alfalfa fields, plant density, height, and percentage of cover were measured. A 0.5-m² sample from each site was cut and taken to the laboratory for measurements of GLAI and wet and dry biomass. Such measurements in cotton and alfalfa fields were made daily for a 7-day period coinciding with the SAR and optical instrument overpasses.

In the early morning after the nighttime ERS-1 SAR overpass, gravimetric soil moisture samples to 5-cm depth were made in selected fields. The bulk density of the soil was computed for each sample based on the volume of the soil sample container and averaged to produce a bulk

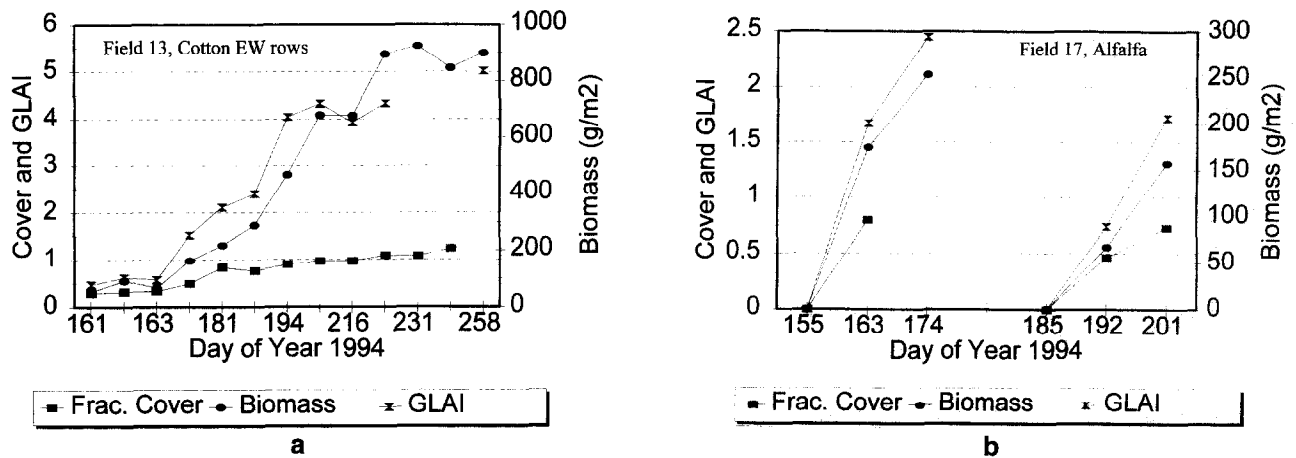


Figure 4. Fractional vegetation cover (V_c) and GLAI for (a) field 13 (cotton) and (b) field 17 (alfalfa) measured in 1994 at MAC.

density estimate for the field. This was used to convert all gravimetric data into values of volumetric soil moisture. Several values were averaged to produce one estimate of soil moisture content for each of the selected borders.

EMPIRICAL RESULTS

Results of an empirical study of the MADMAC data are presented in two sections. First, analysis of the EG&G Daedalus and SNL SAR (Ku band) obtained on 24 June is presented in support of the hypotheses that Ku-band σ^0 is (1) sensitive to soil roughness, (2) sensitive to vegetation density, and (3) insensitive to soil moisture. The sensitivity of Ku-band σ^0 and that of NDVI to vegetation properties are presented, and the limitations of each are discussed. Second, USU optical and ERS-1 SAR (C-band) data obtained on 15 June are presented in support of the hypotheses that C-band σ^0 is (1) sensitive to soil moisture for low biomass levels and (2) sensitive to both soil moisture and vegetation density for high biomass levels. These data are also used to explore the strengths and weaknesses of the relation between C-band σ^0 and T_s .

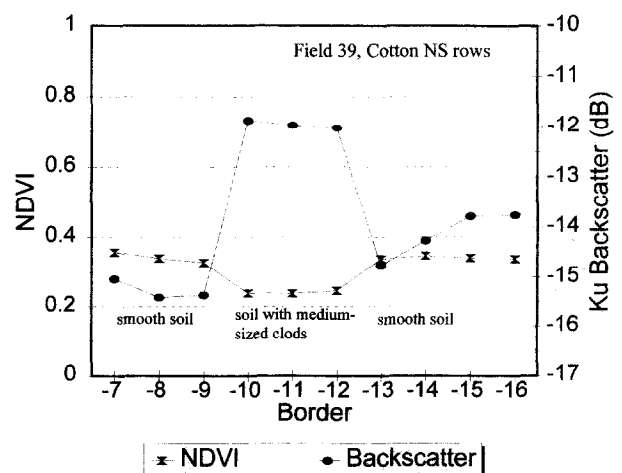
The combined analysis of images acquired over a 10-day period is justifiable. From DOY 165 to 175, the cotton V_c increased from approximately 30% to 50%, and the cotton GLAI increased from approximately 0.6 to 1.7 (Fig. 4a). This increase maintained the partial-cover status of the cotton fields for the combined analysis. The V_c of alfalfa borders was variable but, for most borders on DOY 165, V_c was approximately 80% and GLAI estimates were approximately 1.7. By DOY 175, V_c had increased to 90% and GLAI was as high as 2.4. These conditions allowed analysis of nearly full cover crop conditions on both dates (Fig. 4b). Furthermore, the multi-spectral analysis was segregated into two relatively distinct parts: one associated with the correlation between

NDVI and Ku-band σ^0 (both images acquired on DOY 175) and another associated with the correlation between T_s and C-band σ^0 (both images acquired on DOY 165).

Analysis of Ku-Band σ^0

The Ku-band SAR is theoretically sensitive to variations in surface roughness. For detection of vegetation density for farm management applications, it is desirable to maximize sensitivity to vegetation-related roughness variations and minimize sensitivity to soil roughness. The sensitivity of Ku-band σ^0 to soil roughness is illustrated in field 39. According to qualitative estimates made on DOY 165 (Table 2), the soil roughness within the field varied from "smooth" in borders 7–9 and 13–16 to "cultivated with medium clods" in borders 10–12 (Fig. 5). Although the NDVI in this field changed only slightly

Figure 5. Sensitivity of Ku-band σ^0 to soil roughness in field 39. The soil roughness varied from "smooth" in borders 7–9 and 13–16 to "cultivated with medium clods" in borders 10–12.



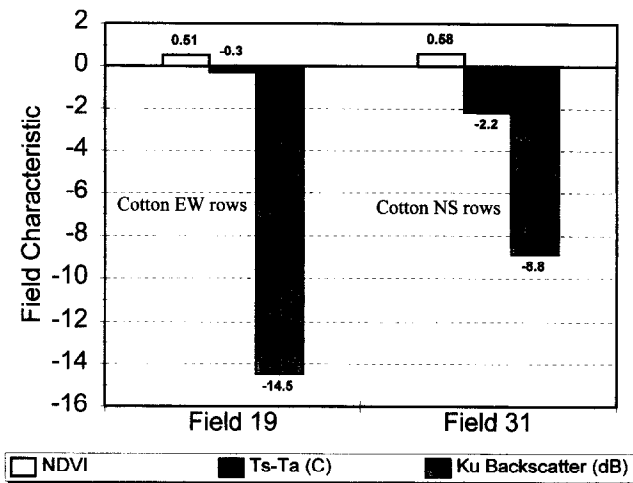


Figure 6. Sensitivity of Ku-band σ^0 to row-furrow orientation in fields 19 and 31. For these cotton fields, the NDVI was similar (0.51 and 0.58), the soil condition was dry, and the row directions were NS for field 31 and EW for field 19.

(from 0.35 to 0.2), the Ku-band σ^0 increased by nearly 4 dB. The clod size in the rough section of field 39 was close to 2 cm (the wavelength of the Ku band), causing the signal to reach a near maximum.

The characteristics of fields 19 and 31 allowed a test of the sensitivity of Ku-band σ^0 row-furrow orientation for partially vegetated fields (Fig. 6). For these cotton fields, the NDVI was similar (0.51 and 0.58), the soil condition was dry (Table 2), and the row directions were north-south (NS) for field 31 and east-west (EW) for field 19. Assuming that the effects of vegetation cover and soil moisture on Ku-band σ^0 were similar, the 5.7-dB difference in the signal could be attributed directly to the difference in row orientation. On the basis of this

Figure 7. Sensitivity of Ku-band σ^0 to variations in vegetation cover (V_c) in fields 23 and 35. For these cotton fields, the within-field soil roughness was constant and V_c varied by border from 20% to 50% in field 23 and from 10% to 30% in field 35.

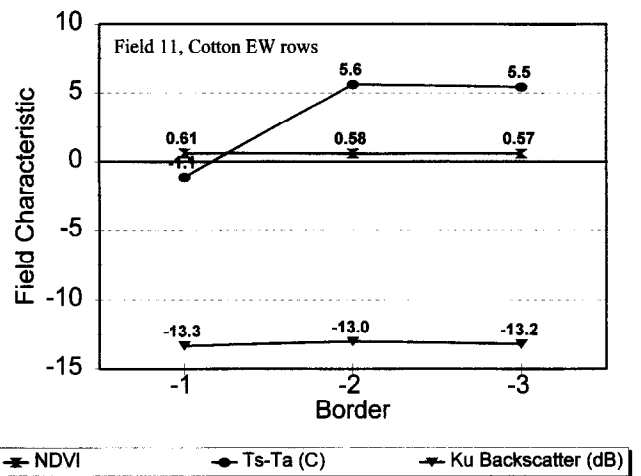
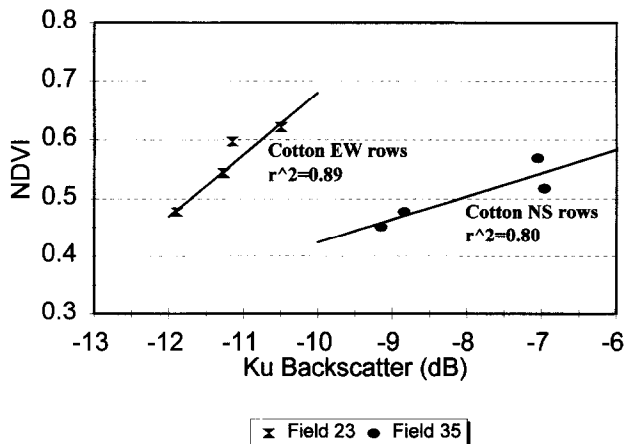


Figure 8. Insensitivity of Ku-band σ^0 to soil moisture in field 11. For this cotton field, the vegetation was relatively uniform (NDVI ranging from 0.57 to 0.61 in three borders), the V_c was low (45%), and the soil moisture ranged from very wet (border 1) to very dry (borders 2 and 3).

observation, cotton fields of similar row orientation were grouped for all further analyses.

To test the sensitivity of Ku-band σ^0 to variations in V_c , two cotton fields of similar soil roughness and varying vegetation cover were selected (Fig. 7). In field 23, the row orientation was EW, the furrows were smooth, and V_c varied from 20% to 50%. In field 35, the row orientation was NS, furrows were raked, and V_c varied from 10% to 30%. Thus, assuming that the soil roughness within the field was uniform, the correlation between NDVI and Ku-band σ^0 could be attributed to the sensitivity of both NDVI and Ku-band σ^0 to vegetation density. The linear regression coefficients of the NDVI-Ku-band σ^0 relations for fields 23 and 35 were 0.89 ($se_x=0.027$, $se_y=0.026$) and 0.80 ($se_x=0.014$, $se_y=0.028$), respectively.

Ku-band σ^0 should be relatively insensitive to soil moisture owing to the lack of surface penetration characteristic of the Ku wavelength (Bouman and Hoekman, 1993). In field 11, the vegetation was relatively uniform (NDVI ranging from 0.57 to 0.61 in three borders), the V_c was low (45%), and the soil moisture ranged from very wet (border 1) to very dry (borders 2 and 3). This variation in soil moisture produced a near 7°C difference in the surface-air temperature (T_s-T_a) but only a 0.3-dB difference in Ku-band σ^0 (Fig. 8). Although the soil moisture difference between the borders was extreme, it elicited little response in the Ku-band σ^0 signal.

Analysis of C-Band σ^0

Although there are many field studies confirming the theoretical relation between C-band σ^0 and soil moisture content for bare soil [e.g., Bertuzzi et al. (1992)], there are few that quantify this relation for vegetated targets.

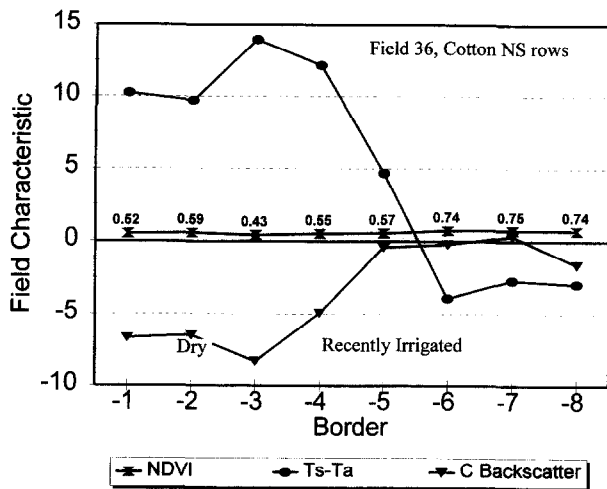


Figure 9. Sensitivity of C-band σ^0 to soil moisture in field 36. For this cotton field, borders 1–3 were dry and borders 5–8 were recently irrigated; the vegetation cover (with the exception of border 3) was about 30% and the GLAI was about 0.7.

The rate of decrease in the sensitivity of C-band σ^0 to soil moisture varies not only with the vegetation density, but also with plant and leaf architecture (Bouman and Kasteren, 1990a, 1990b; Chuah and Tan, 1990; Paris, 1986). Thus, quantifying a universal threshold of V_c for which C-band σ^0 remains sensitive to soil moisture is nearly impossible, though thresholds of $GLAI < 2.0$ have been suggested for common agricultural crops (Ulaby et al., 1984). In field 36, borders 1–3 were dry and borders 5–8 were recently irrigated; the vegetation cover (with the exception of border 3) was estimated to be about 30%. The irrigation in borders 5–8 elicited a drop in $T_s - T_a$ of about 20°C and a rise in C-band σ^0 of 7 dB from the signals for the dry borders (Fig. 9). On the basis of measurements of GLAI and NDVI in other cotton fields, the GLAI of field 36 was estimated to be about 0.7.

The sensitivity of C-band σ^0 to soil moisture for higher GLAI values was tested on the basis of the signal from alfalfa (field 17; $GLAI \sim 1.5$), in which the soil moisture increased from south to north, ranging from 0.09 to 0.32 volumetric soil moisture (m^3/m^3). The C-band σ^0 increased with soil moisture despite the nearly 80% vegetation cover (Fig. 10).

Our results support the results of others who found that the relation between C-band σ^0 and soil moisture was attenuated by increasing V_c . This is also the case for $T_s - T_a$, which has been found to be sensitive to ET rate (a function of both soil moisture and V_c). It follows that C-band σ^0 and $T_s - T_a$ may be related to each other and to ET rate. This hypothesis will be addressed further in the next section.

THEORETICAL JUSTIFICATION

The empirical analysis in the preceding section indicated that multifrequency SAR data obtained for MAC were

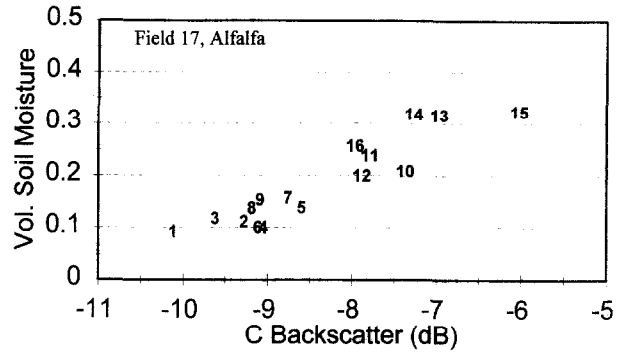


Figure 10. Sensitivity of C-band σ^0 to soil moisture in field 17. For this alfalfa field ($GLAI \sim 1.5$), the soil moisture increased from south to north, (that is, from borders 1 to 16 numbered in the figure) ranging from 0.09 to 0.32 volumetric soil moisture (cm^3/cm^3).

related to two of the most useful optical indices for agricultural farm management. That is, high-frequency radar backscatter was related to the optical NDVI, and low-frequency backscatter was related to $T_s - T_a$. In this section, we propose a physical foundation for these relations based on further analysis of the data and published theories of radiative transfer.

Relation between NDVI and Ku-Band Backscatter

The relation between NDVI and Ku-band σ^0 could be explained by physical theories linking both variables to GLAI. Although NDVI is an "ad hoc prescription" with no explicit physical relation to such vegetation measures as GLAI (Price, 1993), there are canopy radiative transfer models that can determine a reliable relation between NDVI and GLAI [see, e.g., Asrar et al. (1992)]. Price (1992) used such a model to derive a semiempirical relation between a vegetation index (ranging from 0 to 1) and GLAI. We refined this equation to fit the spectral vegetation index NDVI (for which the range depends on the vegetation type) by adding a constant (k), where

$$NDVI = 1 - e^{-(2mGLAI + k)} \quad (3)$$

and m is a coefficient describing the attenuation of radiation as it passes through successive layers of leaves. Both m and k can be determined empirically or theoretically for the crop type of interest. On the basis of a season-long set of spectral and GLAI measurements made for cotton grown at MAC in 1994, Moran et al. (1996b) determined that $NDVI = 1 - e^{[(GLAI + 0.6989)/-2.7290]}$.

The Ku-band σ^0 has also been related directly to GLAI based on a representation of Eq. (2) developed by Attema and Ulaby (1978). According to Eq. (2), the radar signal backscattered by the whole canopy σ^0 is the sum of the contribution of the vegetation σ_v^0 and that of the underlying soil σ_s^0 , where the latter is attenuated by the vegetation layer. Attema and Ulaby (1978) showed that

$$\sigma_v^0 = AV_v^2 \cos^2\theta (1 - \tau^2) \quad (\text{m}^2/\text{m}^2), \quad (4)$$

$$\sigma_s^o = C + Dh_v \text{ (dB)}, \quad (5)$$

h_v is volumetric soil moisture content (cm^3/cm^3), and V_1 is a descriptor of the canopy. τ^2 is the two-way attenuation through the canopy, expressed as

$$\tau^2 = \exp(-2BV_2/\cos\theta) \text{ (unitless)}, \quad (6)$$

where V_2 is a second canopy descriptor. The canopy descriptors (V_1 and V_2) in Eqs. (4) and (6) have been associated with GLAI (Prevot et al., 1993; Ulaby et al., 1984) so, for this application, we assumed $V_1 = V_2 = \text{GLAI}$. Values for A , B , C , and E can be determined by fixing D and minimizing the sum of squares of the differences between modeled and measured σ^o based on Eqs. (4)–(6), where

$$\begin{aligned} \sigma^o = & (AV_1^E \cos\theta \{1 - [\exp(-2BV_2/\cos\theta)]\}) \\ & + [\exp(-2BV_2/\cos\theta)\sigma_s^o] \text{ (m}^2/\text{m}^2). \end{aligned} \quad (7)$$

and σ^o is evaluated with Eq. (5) and converted from units of decibels into square meter per square meter.

For the MADMAC data, Moran et al. (1996c) determined the values of A – E for cotton crops with EW and NS row orientations, resulting in the mesh graph illustrated in Figure 2. They found that, for the Ku-band backscatter (with large incidence angles, acquired at midday), the coefficient $D=0$, indicating that the backscatter was independent of variations in soil moisture content. The Ku-band backscatter is then a function only of calibration coefficients A – C and E and GLAI. This finding was corroborated by the results illustrated in Figure 7.

Thus, the relation found in the preceding section between NDVI and Ku-band backscatter can be described by combining Eqs. (3) and (7) where,

$$\begin{aligned} \text{Ku-band } \sigma^o = & (AV_1^E \cos\theta \{1 - [\exp(-2BV_2/\cos\theta)]\}) \\ & + [\exp(-2BV_2/\cos\theta)C] \text{ (m}^2/\text{m}^2), \end{aligned} \quad (8)$$

where C is converted from units of decibels into square meter per square meter, and $V_1 = V_2 = (-1/2m)[\ln(1 - \text{NDVI}) - k]$ [from Eq. (3)]. It is notable, and unfortunate, that the sensitivities of both Ku-band σ^o and NDVI decrease exponentially with increasing GLAI.

Using the calibration coefficients A – C and E (Moran et al., 1996c) and the m and k coefficients (Moran et al., 1996b), we plotted the MADMAC data with the theoretical shape of the relation between NDVI and Ku-band σ^o defined by Eq. (8) (Fig. 11). These results do not represent an independent validation of this theory, because the coefficients in Eqs. (3) and (7) were obtained from empirical analysis of MADMAC data. However, it does present some support that the relation derived in Eq. (8) adequately portrays the trend of the NDVI–Ku-band σ^o relation.

Relation between $T_s - T_a$ and C-Band Backscatter

The relation between $T_s - T_a$ and C-band σ^o is not as clear as that described for the NDVI and Ku-band σ^o .

In the following discussion, we will show that there is a direct link between $T_s - T_a$ and C-band σ^o for bare soils due to a common sensitivity to soil moisture conditions. However, when vegetation is present, this link becomes more tenuous and complex.

Jackson et al. (1981) wrote the energy balance equation in terms of foliage–air temperature,

$$\begin{aligned} (T_c - T_a) = & [r_a(R_n - G)/C_v] \{ \gamma(1 + r_c/r_a)/[\Delta + \gamma(1 + r_c/r_a)] \} \\ & - \{VPD/[\Delta + \gamma(1 + r_c/r_a)]\}, \end{aligned} \quad (9)$$

where T_c is the crop foliage temperature ($^{\circ}\text{C}$), T_a the air temperature ($^{\circ}\text{C}$), r_a the aerodynamic resistance (s/m), R_n the net radiant heat flux density (W/m^2), G the soil heat flux density (W/m^2), C_v the volumetric heat capacity of air [$\text{J}/(\text{C}^{\circ} \text{m}^3)$], r_c the canopy resistance (s/m) to vapor transport, γ the psychrometric constant (kPa/C°), Δ the slope of the saturated vapor pressure–temperature relation (kPa/C°), and VPD the vapor pressure deficit of the air (kPa). Equation (9) was derived from the Penman–Monteith equation (Allen, 1986), which is limited in application to uniform surfaces, such as full-cover vegetation or bare soil. Moran et al. (1994) proposed that Eq. (9) could be used to determine the surface–air temperatures of saturated bare soil [$(T_s - T_a)_m$] and dry bare soil [$(T_s - T_a)_x$], where subscripts “m” refers to the minimum temperature. Then, for an actual measurement of soil temperature ($T_s - T_a$),

$$E/E_p = [(T_s - T_a) - (T_s - T_a)_x] / [(T_s - T_a)_m - (T_s - T_a)_x], \quad (10)$$

where E is the actual soil surface evaporation rate, E_p is the potential evaporation rate [defined by Allen (1986)], and values of $(T_s - T_a)_m$ and $(T_s - T_a)_x$ (subscript “x” referring to maximum) could be computed from meteorological data based on Eq. (9).

The C-band backscatter is a function of the coefficients A – E and both h_v and GLAI [Eq. (7)]. Unlike Ku-band backscatter, there is a great deal of evidence that $D \gg 0$ for C-band measurements, and thus C-band backscatter is sensitive to soil moisture content [see, e.g., Prevot et al. (1993)]. When $\text{GLAI}=0$, C-band σ^o has been found to have a strong linear relation with soil moisture to depths of 5–7 cm. As GLAI increases, the C-band signal from the soil (σ_s) is attenuated, and the signal from the vegetation component (σ_v) becomes dominant. For the MADMAC data set, Moran et al. (1996c) found that this resulted in the complex curvilinear shape of the near-vertical lines in Figure 2.

Thus, for surfaces with substantial vegetation, it is not feasible to interchange $T_s - T_a$ and C-band σ^o without a priori knowledge of GLAI. However, for bare fields or fields with low vegetation cover, the relation between $T_s - T_a$ and C-band σ^o is direct and robust. When GLAI is zero, Eq. (7) reduces to

$$\text{C-band } \sigma^o = C + Dh_v. \quad (11)$$

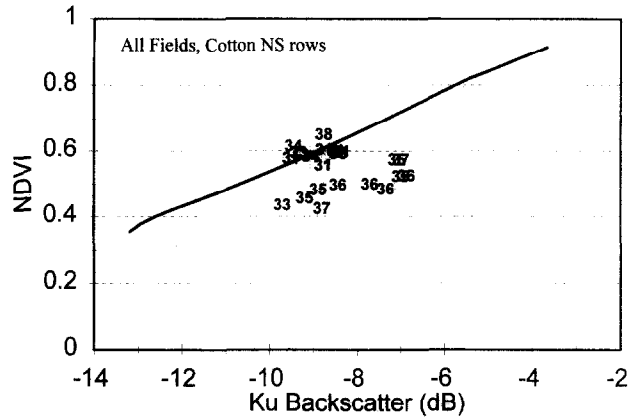
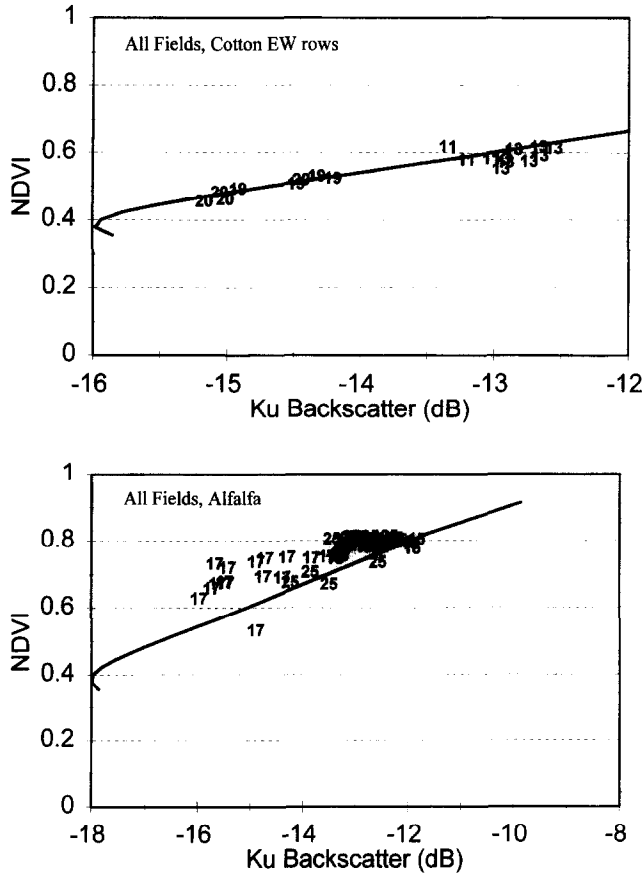


Figure 11. The relation between measurements of Ku-band σ^0 and NDVI for alfalfa fields and cotton fields of similar row direction. Note that field 23 was eliminated from the analysis of cotton fields with EW row orientations because the furrows in this field were smooth, whereas all other field furrows had been raked. The solid line represents the theoretical relation between Ku-band σ^0 and NDVI based on the solution of Eq. (8). The within-figure numbers correspond to the field numbering scheme in Table 2.

According to Eqs. (10) and (11), the link between measurements of $T_s - T_a$ and C-band σ^0 must be based on the relation between E/E_p and h_v .

The relation between E/E_p and h_v for bare soils can be derived from a surface-moisture calculation that is used in mesoscale atmospheric models (McMumber and Pielke, 1981; Tromback and Kessler, 1985). The water potential (Ψ) given by Clapp and Hornberger (1978),

$$\Psi = \Psi_f [h_{vf}/h_v]^b, \quad (12)$$

is used in an expression for the water vapor mixing ratio at the ground surface (r_G) given by Phillip (1957), yielding

$$r_G = e^{[g\Psi/RT]} r_s(T, P), \quad (13)$$

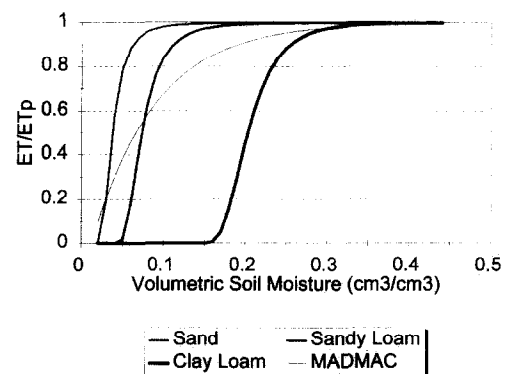
where Ψ is the water potential (m), Ψ_f and h_{vf} are values of moisture potential and volumetric soil moisture content for a soil at saturation, b is a constant dependent on soil type, g is gravity (m/s^2), R is the gas constant for water vapor [$J/(kg K)$], and r_s is the saturation mixing ratio at temperature T and pressure P . They included values of the constants Ψ_f , η_f , and b for various soils, such as sand, sandy loam, and clay loam. Because the ratio $r_G/r_s(T, P)$ is approximately equal to E/E_p , it follows that

$$E/E_p = e^{[g\Psi/RT]}. \quad (14)$$

The form of Eq. (14) was validated empirically for partially vegetated fields (Vidal et al., 1996) with MADMAC measurements of h_v at 5-cm depth, resulting in $(1 - E/E_p) = 1.17e^{[-12.91/h_v]}$ (Fig. 12).

Solving Eqs. (10), (11), and (14) enabled us to derive

Figure 12. The theoretical relation between ET/ET_p and volumetric soil moisture content for three soil types (sand, clay loam, and sandy loam) based on solution of Eq. (14) and the empirical results from MADMAC measurements of partially vegetated fields derived by Vidal et al. (1996).



the shape of the relation between $T_s - T_a$ and C-band σ^0 for bare soil at MAC (Fig. 13). This shape was plotted with the MADMAC data for fields of partial-cover cotton and alfalfa. Although we did not expect the measurements made of vegetated surfaces to coincide with the line derived for bare soil, it was apparent that the theoretical form of the line matched the general trend of the measurements.

CONCLUDING REMARKS

Empirical analysis of the MADMAC data showed that dual-frequency SAR backscatter was related to two of the most useful optical indices for agricultural crop management. That is, high-frequency radar backscatter was related to the optical NDVI, and low-frequency backscatter was related to $T_s - T_a$. Even though the physical mechanisms that caused the radar data to be related to NDVI and $T_s - T_a$ were found to be different from the physical mechanisms that caused NDVI to be related to vegetation density and $T_s - T_a$ to be related to ET rate, it appeared that the optical and microwave data could be interchanged for important agricultural applications.

A theoretical analysis of these optical-SAR relations indicated that there was potential for interchanging NDVI and Ku-band σ^0 for the estimation of crop GLAI.

This relation is strongest for crops with low GLAI, perhaps $GLAI < 3.0$. Such information about crop GLAI would be useful to farm managers for monitoring crop growth and detecting catastrophic events such as insect infestations, crop disease, weed infestations, or water-related stress. Furthermore, GLAI has been found to be the key canopy parameter linking crop growth to multi-spectral reflectance and is the basis of most crop yield models (Bauer, 1985).

We also presented theoretical support for interchanging C-band σ^0 and $T_s - T_a$ for the determination of soil moisture conditions. This theory appears to hold for fields with no vegetation and for fields with very low fractional vegetation cover; that is, fields with GLAI ranging from 0 to 1.0 (Vidal et al., 1996). For many crops, it is necessary to apply a uniform preplanting irrigation and determine the optimum timing for the first postplanting irrigation. Information about soil moisture conditions for these bare soil and near-bare soil conditions could be obtained more frequently by interchanging available measurements of C-band σ^0 and $T_s - T_a$. This approach has a serious limitation related to the depth for which such measurements are correlated directly with soil moisture content. It has been reported that C-band σ^0 is correlated with soil moisture content to depths of 5-7 cm; $T_s - T_a$ may be sensitive to only the surface soil moisture.

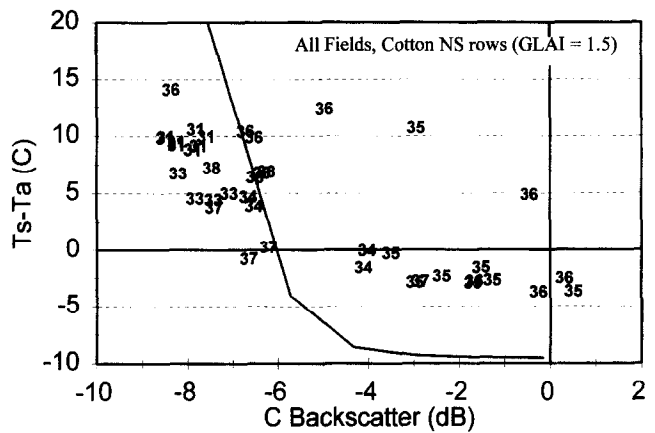
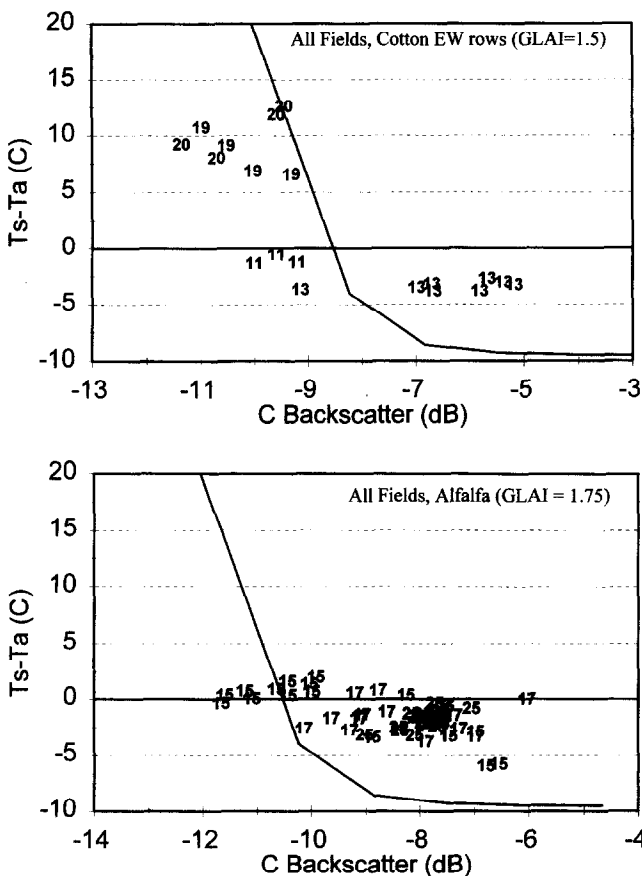


Figure 13. The relation between measurements of C-band σ^0 and $T_s - T_a$ for partially vegetated fields of alfalfa and cotton with similar row directions. The solid line represents the theoretical relation between C-band σ^0 and $T_s - T_a$ for bare soil conditions. The within-figure numbers correspond to the field numbering scheme in Table 2.

Thus, the most likely applications would be for monitoring the uniformity of flood or sprinkler irrigations of bare soils or crops in early growth stages.

A workable satellite-based system for agriculture management might simply use radar backscatter as a surrogate for NDVI and $T_s - T_a$ in current applications. This would require a system in which sensors covering the visible, NIR, thermal, and low- and high-frequency radar were available on a single platform. On clear days, the optical data could provide reliable estimates of field conditions, and the radar could be calibrated on a field-by-field basis with such indices as NDVI and $T_s - T_a$. On cloudy days, the radar data (having been previously calibrated with the optical data) could be interchanged with the optical data to provide the daily information required for most farm management algorithms. This approach would improve both the accuracy of the radar information (through intercalibration) and the frequency of the image acquisition (based on radar cloud penetration). We could possibly achieve the frequency requirements for an ideal crop management system suggested by Jackson (1984); that is, continuous coverage would be optimal with once-a-day coverage as a minimum.

Support for this research was provided by the National Science Foundation (INT-9314872) and by a cooperative grant from the Japanese government. Images were provided by the European Space Agency, Sandia National Laboratories, and EG&G. We express particular appreciation to the Sandia AMPS team who worked with us to arrange the overflights and process the Ku-band SAR images. Dr. Jim Toth (ARS Tucson) provided necessary insights into the relation between evaporation and soil moisture. We also appreciate the cooperation and assistance of personnel at the Maricopa Agricultural Center.

REFERENCES

- Allen, R. G. (1986), A Penman for all seasons. *J. Irrig. Drain. Eng.* 112:348-368.
- Asrar, G., Myneni, R. B., and Choudhury, B. J. (1992), Spatial heterogeneity in vegetation canopies and remote sensing of absorbed photosynthetically active radiation: a modeling study. *Remote Sens. Environ.* 41:85-103.
- Attema, E., and Ulaby, F. (1978), Vegetation modeled as a water cloud. *Radio Sci.* 13:357-364.
- Bauer, M. E. (1985), Spectral inputs to crop identification and condition assessment. *Proc. IEEE* 73:1071-1085.
- Benallegue, M., Normand, M., Galle, S., Dechambre, M., Taconet, O., Vidal-Madjar, D., and Prevot, L. (1994), Soil moisture assessment at a basin scale using active microwave remote sensing: the Agriscatt '88 airborne campaign on the Orgeval watershed. *Int. J. Remote Sens.* 15:645-656.
- Bertuzzi, P., Chanzy, A., Vidal-Madjar, D., and Autret, M. (1992), The use of a microwave backscatter model for retrieving soil moisture over bare soil. *Int. J. Remote Sens.* 13:2653-2668.
- Bouman, B. A. M. (1991), Crop parameter estimation from ground-based X-band (3-cm wave) radar backscattering data. *Remote Sens. Environ.* 37:193-205.
- Bouman, R. A. M., and Hoekman, D. H. (1993), Multi-temporal, multi-frequency radar measurements of agricultural crops during the Agriscatt-88 campaign in The Netherlands. *Int. J. Remote Sens.* 14:1595-1614.
- Bouman, R. A. M., and van Kasteren, H. W. J. (1990a), Ground-based X-band (3-cm wave) radar backscattering of agricultural crops I: sugar beets and potato; backscattering and crop growth. *Remote Sens. Environ.* 34:93-105.
- Bouman, B. A. M., and van Kasteren, H. W. J. (1990b), Ground-based X-band (3-cm wave) radar backscattering of agricultural crops II: wheat, barley and oats; the impact of canopy structure. *Remote Sens. Environ.* 34:107-118.
- Brisco, B., Brown, R. J., Koehler, J. A., Sofko, G. J., and McKibben, M. J. (1990), The diurnal pattern of microwave backscattering by wheat. *Remote Sens. Environ.* 34:37-47.
- Brown, R. J., Manore, M. J., and Poirier, S. (1992), Correlations between X-, C-, and L-band imagery within an agricultural environment. *Int. J. Remote Sens.* 13:1645-1661.
- Carlson, T. N., Gillies, R. R., and Perry, E. M. (1994), A method to make use of thermal infrared temperature and NDVI measurements to infer surface soil water content and fractional vegetation cover. *Remote Sens. Rev.* 9:161-173.
- Chuah, H. T., and Tan, H. S. (1990), A multiconstituent and multilayer microwave backscatter model for a vegetative medium. *Remote Sens. Environ.* 31:137-153.
- Clapp, R., and Hornberger, G. (1978), Empirical equations for some soil hydraulic properties. *Water Resour. Res.* 14:601-604.
- Dabrowska-Zielinska, Gruszczynska, K., Janowska, M., Stankiewicz, K., and Bochenek, Z. (1994), Use of ERS-1 SAR data for soil moisture assessment. In *Proc. Second Euro-Latin American Space Days*, pp. 79-84, 9-13 May, Buenos Aires, Argentina.
- Daughtry, C. S. T., Ranson, K. J., and Biehl, L. L. (1991), C-band backscattering from corn canopies. *Int. J. Remote Sens.* 12:1097-1109.
- Engman, E. T. (1991), Applications of microwave remote sensing of soil moisture for water resources and agriculture. *Remote Sens. Environ.* 35:213-226.
- Fung, A. K., and Chen, K. S. (1992), Dependence of the surface backscattering coefficients on roughness, frequency and polarization states. *Int. J. Remote Sens.* 13:1663-1680.
- Hope, A. S. (1988), Estimation of wheat canopy resistance using combined remotely sensed spectral reflectance and thermal observations. *Remote Sens. Environ.* 24:369-383.
- Huete, A. R. (1988), A soil-adjusted vegetation index (SAVI). *Remote Sens. Environ.* 25:89-105.
- Idso, S. B., Clawson, K. L., and Anderson, M. G. (1986), Foliage temperature: effects of environmental factors with implications for plant water stress assessment and the CO₂/climate connection. *Water Resour. Res.* 22:1702-1716.
- Jackson, R. D. (1982), Canopy temperature and crop water stress. *Adv. Irrig.* 1:43-85.
- Jackson, R. D. (1984), Remote sensing of vegetation characteristics for farm management. *SPIE Remote Sens.* 475:81-96.
- Jackson, R. D. (1987), The crop water stress index: a second look. In *Proc. Int. Conf. on Measurement of Soil and Plant Water Status*, Utah State Univ., 6-10 July, Logan, UT.

- Jackson, R. D., and Huete, A. R. (1991), Interpreting vegetation indices. *Prev. Vet. Med.* 11:185–200.
- Jackson, R. D., Idso, S. B., Reginato, R. J., and Pinter, P. J., Jr. (1981), Canopy temperature as a crop water stress indicator. *Water Resour. Res.* 17:1133–1138.
- Lagouarde, J. P., Kerr, Y. H., and Brunet, Y. (1995), An experimental study of angular effects on surface temperature for various plant canopies and bare soil. *Agric. For. Meteorol.* 77:167–190.
- Lin, D. S., Wood, E. F., Beven, K., and Saatchi, S. (1994), Soil moisture estimation over grass-covered areas using AIRSAR. *Int. J. Remote Sens.* 15:2323–2343.
- McCumber, M. C., and Pielke, R. A. (1981), Simulation of the effects of surface fluxes of heat and moisture in a mesoscale numerical model I: soil layer. *J. Geophys. Res.* 86:9929–9938.
- Moran, M. S. (1994), Irrigation management in Arizona using satellites and airplanes. *Irrig. Sci.* 15:35–44.
- Moran, M. S., Clarke, T. R., Qi, J., and Pinter, P. J., Jr. (1996a), MADMAC: a test of multispectral airborne imagery as a farm management tool. In *Proc. 26th Int. Symp. on Remote Sensing of the Environment*, pp. 612–617, 25–29 March, Vancouver, BC, Canada.
- Moran, M. S., Clarke, T. R., Inoue, Y., and Vidal, A. (1994), Estimating crop water deficit using the relation between surface-air temperature and spectral vegetation index. *Remote Sens. Environ.* 49:246–263.
- Moran, M. S., Maas, S. J., Clarke, T. R., Pinter, P. J., Jr., Qi, J., Mitchell, T. A., Kimball, B. A., and Neale, C. M. U. (1996b), A modeling/remote sensing approach for irrigation scheduling. In *Proc. Int. Symp. on Evaporation and Irrigation Scheduling*, pp. 679–684, 3–6 Nov. 1996, San Antonio, TX.
- Moran, M. S., Vidal, A., Troufleau, D., Inoue, Y., and Mitchell, T. (1996c), Modeling multi-frequency microwave data for farm management in Arizona. *IEEE Trans. Geosci. Remote Sens.*, in press.
- Neale, C. M. U., and Crowther, B. G. (1994), An airborne multispectral video/radiometer remote sensing system: development and calibration. *Remote Sens. Environ.* 49:187–194.
- Nemani, R. R., and Running, S. W. (1989), Estimation of regional surface resistance to evapotranspiration from NDVI and thermal-IR ADHRR data. *J. Appl. Meteorol.* 28:276–284.
- Paris, J. F. (1986), The effect of leaf size on the microwave backscattering by corn. *Remote Sens. Environ.* 19:81–95.
- Phillip, J. (1957), Evaporation, and moisture and heat fields in the soil. *J. Meteorol.* 14:354–366.
- Poirier, S., Thomson, K. P. B., Condal, A., and Brown, R. J. (1988), SAR applications in agriculture: a comparison of steep and shallow mode (30° and 53° incidence angles) data. *Int. J. Remote Sens.* 10:1085–1092.
- Prevot, L., Champion, I., and Guyot, G. (1993), Estimating surface soil moisture and leaf area index of a wheat canopy using dual-frequency (C and X bands) scatterometer. *Remote Sens. Environ.* 46:331–339.
- Price, J. C. (1990), Using spatial context in satellite data to infer regional scale evapotranspiration. *IEEE Trans. Geosci. Remote Sens.* GE-28:940–948.
- Price, J. C. (1992), Estimating vegetation amount from visible and near infrared reflectances. *Remote Sens. Environ.* 41:29–34.
- Price, J. C. (1993), Estimating leaf area index from satellite data. *IEEE Trans. Geosci. Remote Sens.* 31:727–734.
- Qi, J., Moran, M. S., Cabot, F., and Dedieu, G. (1995), Normalization of sun/view angle effects on vegetation indices with bidirectional reflectance function models. *Remote Sens. Environ.* 52:207–217.
- Rouse, J. W., Haas, R. H., Schell, J. A., Deering, D. W., and Harlan, J. C. (1974), Monitoring the vernal advancement and retrogradation (greenwave effect) of natural vegetation. *NASA Goddard Space Flight Center Type III Final Report*, Greenbelt, MD.
- Schmullius, C., and Furrer, R. (1992a), Frequency dependence of radar backscattering under different moisture conditions of vegetation-covered soil. *Int. J. Remote Sens.* 13:2233–2245.
- Schmullius, C., and Furrer, R. (1992b), Some critical remarks on the use of C-band radar data for soil moisture detection. *Int. J. Remote Sens.* 13:3387–3390.
- Soares, J. V., Bernard, R., and Vidal-Madjar, D. (1987), Spatial and temporal behavior of a large agricultural area as observed from airborne C-band scatterometer and thermal infrared radiometer. *Int. J. Remote Sens.* 8:981–996.
- Tanner, C. B. (1963), Plant temperature. *Agron. J.* 55:210–211.
- Tremback, C. J., and Kessler, R. (1985), A surface temperature and moisture parameterization for use in mesoscale numerical models. *Proc. 7th Conf. on Numerical Weather Prediction*, 17–20 June, Montreal, Quebec, Canada.
- Troufleau, D., Vidal, A., Beaudoin, A., Moran, M. S., Weltz, M. A., Goodrich, D. C., Washburne, J., and Rahman, A. F. (1997), Using optical and microwave synergy for estimating surface energy fluxes over semi-arid rangeland. *Remote Sens. Rev.* (in press).
- Ulaby, F. T., Allen, C. T., Eger, G., III, and Kanemasu, E. (1984), Relating the microwave backscattering coefficient to leaf area index. *Remote Sens. Environ.* 14:113–133.
- Vidal, A., and Devaux-Ros, C. (1995), Evaluating forest fire hazard with a Landsat TM derived water stress index. *Agric. For. Meteorol.* 77:207–224.
- Vidal, A., Troufleau, D., Moran, M. S., and Qi, J. (1996), Crop evapotranspiration estimation using optical and microwave remote sensing. In *Proc. Int. Symp. on Evaporation and Irrigation Scheduling*, pp. 231–238, 3–6 November, 1996, San Antonio, TX.